


RESEARCH ARTICLE

AlGaAs/Si dual-junction tandem solar cells by epitaxial lift-off and print-transfer-assisted direct bonding

Kanglin Xiong^{1,*}, Hongyi Mi^{1,*}, Tzu-Hsuan Chang^{1,*}, Dong Liu^{1,*} , Zhenyang Xia¹, Meng-Yin Wu², Xin Yin², Shaoqin Gong³, Weidong Zhou⁴, Jae Cheol Shin⁵, Xiuling Li⁶, Michael Arnold², Xudong Wang², Hao-Chih Yuan⁷ & Zhenqiang Ma¹

¹Department of Electrical and Computer Engineering, University of Wisconsin-Madison, Madison Wisconsin, 53706

²Department of Material Science and Engineering, University of Wisconsin-Madison, Madison, Wisconsin 53706

³Department of Biomedical Engineering, University of Wisconsin-Madison, Madison, Wisconsin 53706

⁴Department of Electrical Engineering, University of Texas-Arlington, Arlington, Texas 76019

⁵Department of Physics, Yeungnam University, 280 Dae-dong, Gyeongsan 712-749, Korea

⁶Department of Electrical and Computer Engineering, University of Illinois at Urbana-Champaign, Urbana, Illinois 61801

⁷National Renewable Energy Lab, Golden, Colorado 80401

Keywords

Epitaxy, heterogeneous, solar cell, thin films

Correspondence

Zhenqiang Ma, Department of Electrical and Computer Engineering, University of Wisconsin-Madison, Madison, WI 53706.

E-mail: mazq@engr.wisc.edu

and

Hao-Chih Yuan, National Renewable Energy Lab, Golden, CO 80401. E-mail: haochih.yuan@gmail.com

Funding Information

The work was supported by AFOSR under a PECASE grant FA9550-09-1-0482.

Received: 26 September 2017; Revised: 28 November 2017; Accepted: 29 November 2017

Energy Science and Engineering 2018; 6(1): 47–55

doi: 10.1002/ese3.182

*The authors contributed equally.

Introduction

The development and utilization of solar energy have steadily evolved in the past decades. As traditional homogeneous solar cells, made of Si, III-V, and organic materials, have approached their physical limits, perovskites [1–4] and multijunction solar cell techniques that feature higher efficiency, lower cost, and capabilities of integrating heterogeneous solar cells have been explored to broaden spectrum utilization for next-generation solar cells [5]. Among them, III-V/Si multijunction solar cells are of great

Abstract

A novel method is developed to realize a III-V/Si dual-junction photovoltaic cell by combining epitaxial lift-off (ELO) and print-transfer-assisted bonding methods. The adoption of ELO enables III-V wafers to be recycled and reused, which can further lower the cost of III-V/Si photovoltaic panels. For demonstration, high crystal quality, micrometer-thick, GaAs/AlGaAs/GaAs films are lifted off, transferred, and directly bonded onto Si wafer without the use of any adhesive or bonding agents. The bonding interface is optically transparent and conductive both thermally and electrically. Prototype AlGaAs/Si dual-junction tandem solar cells have been fabricated and exhibit decent performance.

interest in the photovoltaic field. Due to the optical and electrical properties of III-V materials, homogeneous epitaxial III-V solar cells exhibit exceptional performance in terms of energy conversion efficiency [6]. Contrary to III-V solar cells, single crystal Si solar cells have already been widely adopted by utility solar plants and rooftop applications due to the low cost of Si wafers. Although Si solar cells have gained significant advancement in markets over the decades, the efficiency of the Si solar cells is limited by the thermal relaxation of hot carriers. With the motivation of cost reduction and solar energy

conversion efficiency improvement, the combination of III-V with Si for photovoltaics have been explored by researchers to fully take advantage of the complementary benefits of each individual cell. Furthermore, epitaxial III-V materials of only a few micrometers thick will be needed in the photovoltaic process; therefore, the material cost of the epitaxy seeding wafers could be significantly reduced by III-V thin-film transfer and wafer recycling. Second, Si with robust mechanical strength and high thermal conductivity can provide reliable support and heat dissipation for III-V solar cells. Moreover, regarding solar spectrum absorption, the 1.12 eV bandgap of Si makes it a good complementary junction in tandem with III-V materials. In light of these advantages, numerous endeavors have been dedicated to the pursuit of high-quality III-V/Si using different approaches.

Direct growth is one of the most intuitive approaches. However, the challenges of directly epitaxial growth of high-quality III-V materials on Si substrate still remain unsolved. The main problem arises from a 4% lattice mismatch between GaAs and Si, and the disparity in thermal expansion coefficient between III-V and Si. Besides, the transition from nonpolar Si to polar III-V materials could introduce an antiphase domain [7, 8]. The AlGaAs/Si dual-junction solar cell [9] and GaInP/GaAs tandem solar cells on nonactive Si carrier have been demonstrated [10]. However, the performance is still affected by the short minority carrier diffusion length resulting from over $10^7/\text{cm}^2$ dislocation density despite the thick buffer layer used. To circumvent the problem with heterogeneous growth of III-V on Si, a thin layer of single crystal nucleation layer such as InP and GaAs have been transferred onto Si by wafer bonding and lift-off. Subsequently, III-V solar cells are grown on the InP/Si or GaAs/Si solar cells [11, 12]. However, these processes not only complicate fabrication, but also suffer from cracks in the III-V thin film due to thermal strain during growth.

As an alternative, wafer bonding allows the homogeneous epitaxial growth of high-performance solar cell on its natural substrate. Once two wafers are bonded together, one of the wafers can be removed by wet chemicals. The direct bonding of GaInP/GaAs on GaAs and GaInAsP/GaInAs on InP yield four-junction solar cells with world record efficiency for concentration application [13]. There is also ongoing research on the bonding of III-V to Si for solar cells, which mainly focuses on low temperature, interface optical transparency, and thermal and electrical conductivity [14–16]. Surface-activated direct bonding at room temperature avoids high-temperature annealing and GaInP/GaAs/Si triple-junction solar cells are demonstrated [17]. Direct fusion bonding under a low postbonding temperature of 500°C or less has been investigated and a dual-junction AlGaAs/Si has been fabricated, where two

full wafers were consumed for the fabrication [18]. Nondirect bonding, which used metal or carbon nanotube agents, would sacrifice the interface properties and therefore is not optimal for photovoltaic application [19, 20]. It has been noticed that among the abovementioned wafer-bonding processing techniques, the top III-V wafer is usually etched away after bonding to expose the top solar cells, which inevitably increases the cost of solar cell fabrication.

In contrast, epitaxial lift-off III-V films and solar cells by using sacrificial layers and etchants have been engineered so that the III-V wafers can be reused [21–23]. The released freestanding III-V nanomembrane can form van der Waals forces with a variety of substrates with the help of capillary force from water [24]. Recently, with As_2Se_3 as the bonding agent, triple-junction GaInP/GaAs/InGaAsNSb epitaxially grown solar cells have been bonded onto Ge solar cells after being released from the GaAs wafer [25].

In this paper, we realized the III-V/Si tandem solar cell by ELO and print-transfer-assisted direct bonding methods. As expected, after combining with Si cell, the obtained tandem solar cell demonstrates better performance than that of individual III-V thin-film cell and Si cell. In addition, compared with bonding by adhesion, our direct bonding adopts the electrically conductive interface so that two tandem solar cells are monolithically integrated together. In this way, the approach circumvents problems such as heat dissipation of III-V solar cells and light shadowing from the adhesion layers. Meanwhile, the III-V carrier wafer can be recycled for another ELO growth, which can significantly reduce the material cost per cell.

Experiments and Results

ELO and print-transfer bonding

The step-by-step polydimethylsiloxane (PDMS)-assisted printing transfer process is shown in Figure 1 [26]. To begin with, a GaAs/AlGaAs/GaAs/AlAs layer was homogeneously epitaxially grown on a GaAs handling substrate (Fig. 1A) with a special 1- μm AlAs interlayer (Fig. 1B) [27]. This AlAs interlayer, or so-called sacrificial layer, can be selectively etched away by a gas or liquid etchant, while the top functional III-V film remains intact. The undercut etching of the sacrificial layer in liquid involves chemical reactions, dissolution of by-products, and mass transport [21, 28, 29]. The undercut etching can be affected by many factors such as the geometry of the sample, the concentration of etchant, and the chemical composition of the sacrificial layer. Although the undercut can be done on wafer scale to obtain a large freestanding III-V film [23, 30], a prepatterned substrate with exposed undercut layer can significantly reduce the undercut time,

as shown in Figure 1C and D. After the undercut etching, the freestanding III-V film is ready to be picked up and applied in a variety of applications.

III-V thin film was thereafter transferred onto Si wafer by a controllable printing method, while the remaining GaAs substrate were recycled and reused (Fig. 1A–E). First, a PDMS stamp was used to pick up the III-V film from the undercut epitaxial wafer (Fig. 1F). Then, the stamp was printed with the III-V film onto the target Si wafer (Fig. 1G). Finally, removal of the PDMS stamp yielded the III-V/Si bonding (Fig. 1H and I). No bonding or adhesive agents were used in this process. The bonding strength exclusively depends on the van der Waals forces between the surfaces of the III-V and Si. The thicker the membrane, the higher the difficulty for the membrane to stay conformally on an uneven target surface. Moreover, due to residual strain, the III-V film may curve up and fail to bond with the Si surface. Thus, to ensure strong bonding strength, the two contact surfaces must be very smooth and clear of particles. For III-V film of a few micrometers thick in photovoltaic applications, the requirement for an immaculate surface is stringent to achieve successful bonding.

By employing direct bonding to form the heterojunction, both light scattering and light absorption at the heterogeneous interface can be minimized, while heat dissipation of solar cells remains efficient. With proper III-V material and doping concentration, the III-V/Si interface can be made very conductive [17]. Photocurrent can flow vertically across the interface instead of laterally within the base and emitter layers. Thus, there is no current spreading issue at the base of the top junction and the emitter of the bottom junction.

In the following section, the design, fabrication, and performances characteristics of dual-junction solar cells made of micrometer-thick III-V film bonded with Si bottom cell wafer are described in detail.

Tandem solar cell design

The Shockley–Queisser efficiency [31] of a dual-junction tandem solar cell depends on the bandgap of each junction shown in Figure 2A. Due to the current matching constraint and relaxation of hot carriers, the favored bandgap combination is limited to a very small range with a bandgap of 1.12 eV. Si works the best with materials with a bandgap of ~ 1.8 eV, according to Figure 2A. Therefore, $\text{Al}_{0.3}\text{Ga}_{0.7}\text{As}$ with a bandgap of 1.8 eV was selected as the top cell in our work to approximate the efficiency optima shown in Figure 2A.

A schematic diagram of the structure of the dual-junction solar cell is shown in Figure 2B along with a detailed illustration of the layer thicknesses and doping concentrations of the two cells. The additional p^{++} GaAs bottom layer of the top cell is designed to form a tunneling junction with the n^{++} emitter of the bottom Si cell, thus electrically connecting the top AlGaAs and bottom Si cells.

Transfer AlGaAs onto Si

The bottom Si solar cell was fabricated prior to the GaAs/AlGaAs/GaAs transfer as Si solar cell fabrication involves high-temperature processes. The n^{++} emitter was formed on a 300- μm -thick, double-side polished p-type Si wafer by POCl_3 gas-phase diffusion. The degenerated

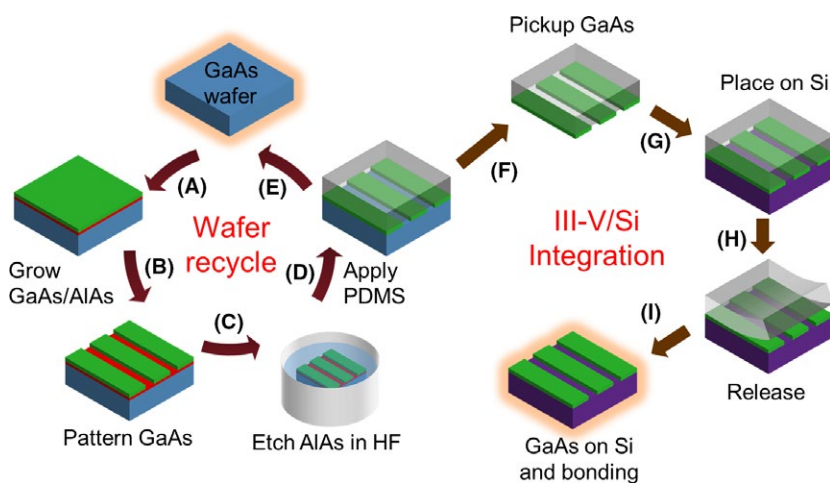


Figure 1. Schematic process flow of the epitaxial layer growth, release, transfer, bonding, and wafer recycle for III-V/silicon integration. (A) Begin with a bare GaAs wafer. (B) Epitaxial growth of GaAs/AlGaAs/GaAs/AlAs layer on top of the eGaAs wafer. (C) Patterning of GaAs/AlGaAs/GaAs layer using photolithography. (D) Selective etching of AlAs in HF. (E) Application of PDMS onto the released layer. (F) Pick up of the released GaAs/AlGaAs/GaAs layer. (G) Transfer of the GaAs/AlGaAs/GaAs layer to Si. (H) Release of PDMS stamp. (I) Thermal anneal to finish chemical bonding.

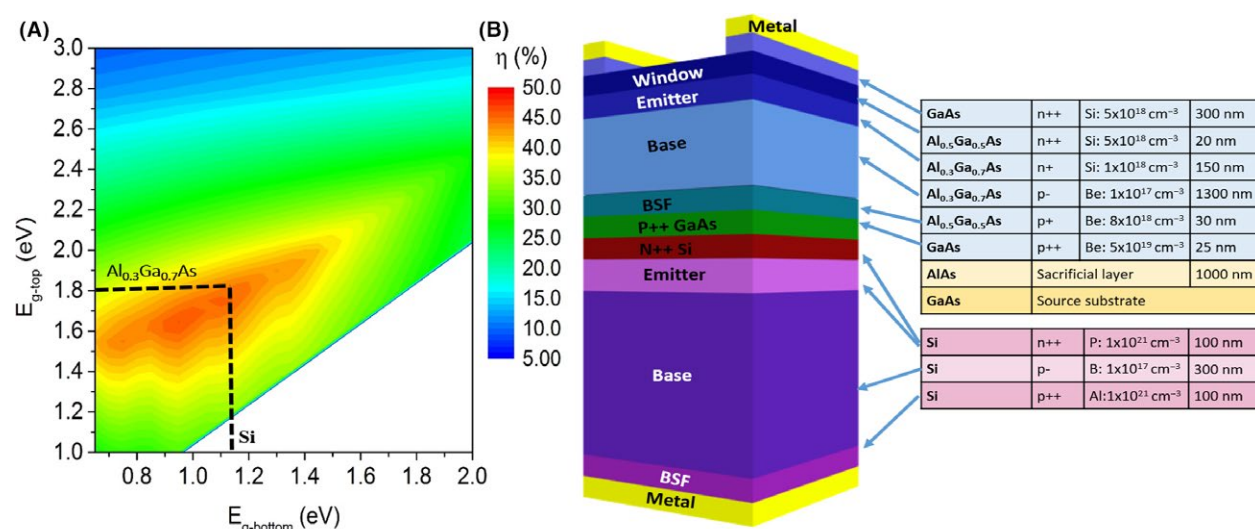


Figure 2. (A) Using Shockley–Queisser efficiency limit to illustrate the optimal efficiency of AlGaAs ($E_g = 1.8$ eV)–Si ($E_g = 1.12$ eV) dual-junction solar cells. (B) Schematic structure of the dual-junction tandem $Al_{0.3}Ga_{0.7}As/Si$ solar cell along with the detailed layer structures of the two cells.

phosphorus-doped top surface forms the conductive tunneling junction when contacted with the transferred p^{++} GaAs layer. Annealing of the Al paste on the backside of the Si forms the back surface field (BSF) and ohmic contact.

The AlGaAs solar cell with n^{+} GaAs contact layer on top and a p^{++} GaAs layer at the bottom was grown on top of a sacrificial AlAs layer on a GaAs substrate by MOCVD (Fig. 2B). The two GaAs layers sandwiching the AlGaAs structure serve as protection during wet etching. The wafer was then patterned into strips by inductively coupled plasma (ICP) etching to expose the AlAs layer. ELO of the n/p GaAs/AlGaAs/GaAs structure was implemented by undercutting the AlAs sacrificial layer with hydrofluoric acid (HF). The lateral etching selectivity of AlAs over the AlGaAs layer in highly diluted HF is over 50, which is sufficient to lift off AlGaAs strips of several hundreds of micrometers wide. Figure 3A shows a cross-sectional scanning electron microscope (SEM) image of the 1.8- μm -thick top cell film suspended on a partially undercut AlAs sacrificial layer. For a 250- μm -wide strip, it takes about 2 h in 1:250 diluted HF to finish the undercut. There is no restriction for the length of the strips, as strips of a few millimeters long have been successfully lifted off.

After the complete undercut of AlAs, the GaAs/AlGaAs/GaAs strips were picked up by a PDMS stamp, and HF residual is then removed by rinsing the undercut sample with deionized (DI) water several times. To facilitate the bonding between the two materials, clean, smooth, and particle-free surfaces are prerequisite for both sides. As shown in the microscope picture of Figure 3B, the

backside of the AlGaAs strips was very clean. The surface quality of the backside of the AlGaAs strip and Si cell top were both confirmed by atomic force microscopy (AFM) measurements that indicate a RMS roughness < 2 nm (Fig. 3C and D). The AlGaAs strips were then transferred onto the Si cell using a print-transfer method without the use of adhesive or bonding agents. The top view optical microscopic image of the resulting AlGaAs/Si is shown in Figure S1A. The AlGaAs remains bonded to the Si surface due to van der Waals forces between the p^{++} GaAs and n^{++} Si surfaces. Although there is strain in the 1.8- μm -thick GaAs/AlGaAs/GaAs structure, its bonding with Si is feasible. The bonding process was carried out in class 10 lithography bay in clean room to minimize particles. To further strengthen the bonding, the sample was baked on a hot plate, followed by annealing in nitrogen ambient at a temperature in the range of 200–500°C. The AlGaAs cell annealed at 500°C remained conformal to the Si surface, as shown in Figure S1B. Zoom-in cross-sectional SEM images in Figure S1B clearly show the multiple layers of the AlGaAs/Si tandem solar cell. Figure S1C shows the transmission electron microscopy image of the cross-section of the bonded p^{++} GaAs/ n^{++} Si heterojunction interface, together with band structure at equilibrium by simulation. There is an amorphous layer between the single crystal GaAs and Si that is around 3.5 nm as shown in Figure 3E. A series of selected area electron diffraction patterns for Si, GaAs, and the area close to GaAs/Si heterojunction interface are shown in Figure 3F–H. These diffraction patterns verify that the GaAs and Si above and below the amorphous layer were a perfect single crystal. These observations imply that the

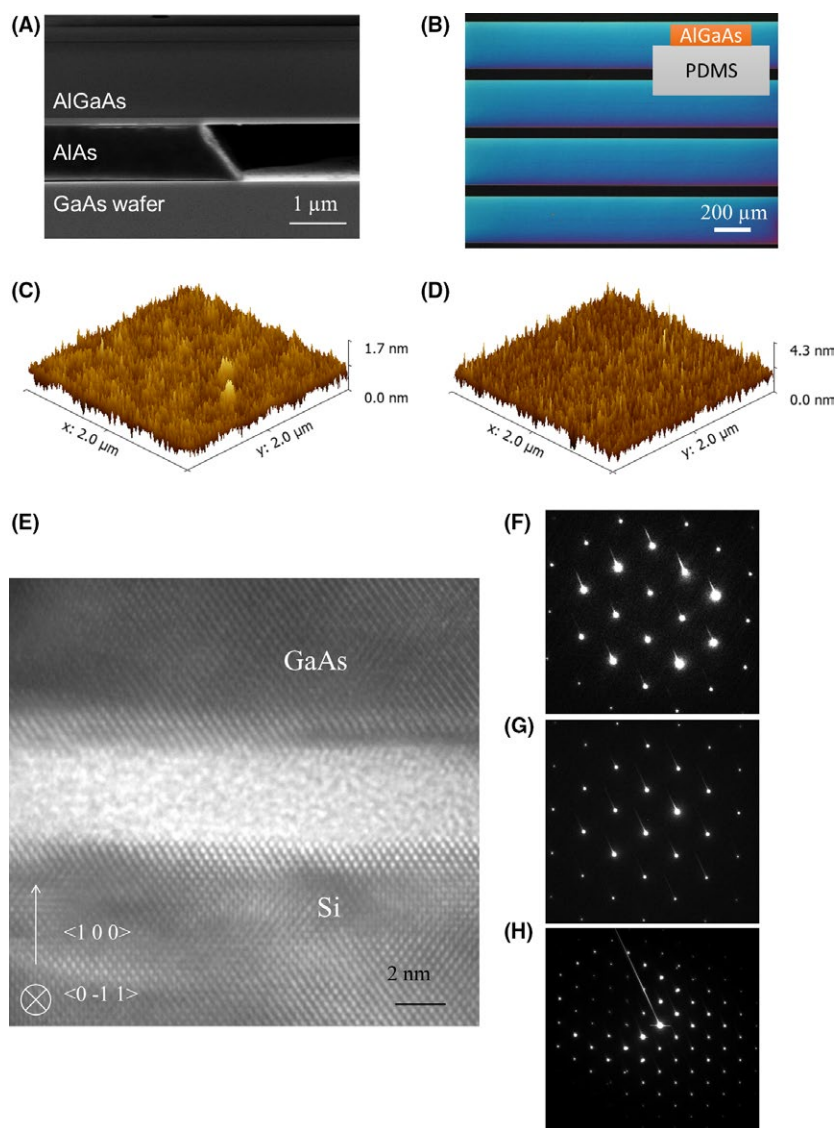


Figure 3. Cross-sectional SEM images of a partially undercut sample. (A) The top 1.8 μm GaAs/AlGaAs/GaAs layer suspended after the AlAs beneath was etched. (B) Optical image of the backside of PDMS where the top GaAs/AlGaAs/GaAs layer evenly adhered to the step after the pick-up step (Fig. 1F). (C) AFM roughness mapping for the backside surface of the GaAs of the released GaAs/AlGaAs/GaAs layer. (D) AFM roughness mapping for the top surface of the bottom Si cell. (E) Cross-sectional transmission electron microscope (TEM) image of the GaAs/Si heterojunction. Selected area electron diffraction patterns for (F) Si, (G) GaAs, and (H) a region near the GaAs/Si heterojunction interface.

single crystal quality of GaAs and Si was not compromised during the ELO-transfer-assisted bonding process and there was no clear lattice distortion dislocation around the bonded heterojunction. The electrical characterization of the $\text{p}^{++}\text{GaAs}/\text{n}^{++}\text{Si}$ conductive heterojunction formed by the ELO-transfer-assisted bonding is shown in Figure S2D.

The crystal quality of transferred III-V film on target Si wafer is further verified by X-ray diffraction (XRD). Along with the GaAs wafer peak, the triple crystal (004) $\omega/2\theta$ scan of epitaxial wafer shows the peak of the AlGaAs

layer and the AlAs sacrificial layer, as shown in Figure 4A. The Al content ratio is 0.3 and 1.0, respectively. After GaAs/AlGaAs/GaAs was transferred onto Si, the AlAs peak disappeared. The GaAs cap layer peak was weaker than the AlGaAs peak because it is relatively thinner. Figure 4B shows the (004) reciprocal space mapping (RSM), where the AlGaAs (100) is about 1.5 degree offset to the Si (100) due to GaAs epitaxial substrate miscut. The (224) RSM in Figure 4C shows that the GaAs contact layer remains coherent with the AlGaAs layer after ELO and print transfer.

Results and Discussion

After the bonding of AlGaAs with Si, the dual-junction tandem solar cells were fabricated using conventional methods. The Al contact on the bottom of Si could be etched by photoresist developers and acids; thus, these parts must be covered by photoresist during certain processing steps. The AlGaAs window, base, and bottom Si

emitter were exposed by plasma etching. For the four terminal tandem solar cells as shown in Figure 5B, the AuGe/Ni/Au, Ti/Pt/Au, and Ni/Au metal contacts were deposited by e-beam evaporator onto the GaAs contact layer, AlGaAs base, and n^{++} Si emitter, respectively. For two-terminal tandem solar cells depicted in Figure 5C and D, only the AuGe/Ni/Au contact was deposited on the GaAs contact layer, and the Al paste at the backside

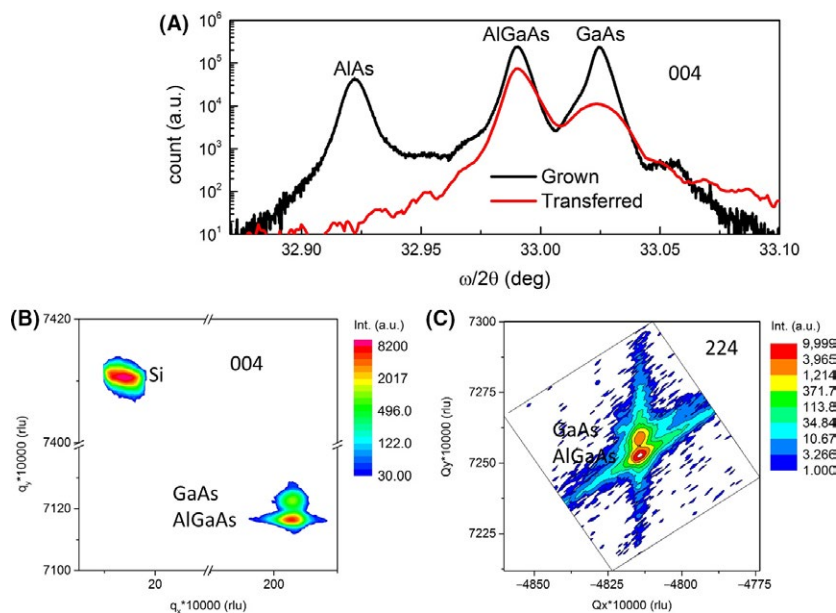


Figure 4. (A) X-ray diffraction spectra for the grown layer of GaAs/AlGaAs/GaAs/AlAs on a GaAs substrate (black) and transferred GaAs/AlGaAs/GaAs layer on the Si bottom cell (red). (B) Reciprocal space mapping (RSM) (004) of transferred GaAs/AlGaAs/GaAs layer on the Si bottom cell. (C) RSM (224) for the AlGaAs cell and GaAs contact layer indicating the coherent existence of the two epi layers.

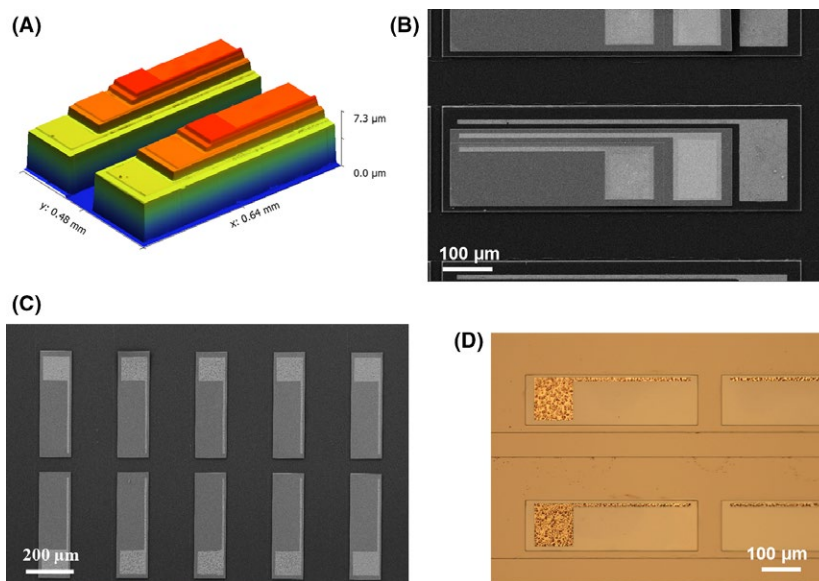


Figure 5. (A) 3D structure of finished AlGaAs/Si tandem solar cell scanned by Zygo white light interferometer. SEM image of a top view of (B) four-terminal tandem solar cells and (C) two-terminal tandem solar cell. (D) Optical microscopic image of the top view of two-terminal tandem solar cells.

of Si wafer serves as the ground contact. The isolation between cells is accomplished by dry etching. Note that the AlGaAs film stayed on Si during the process, including the contact annealing, even though the metal alloying process may introduce strains.

The finished solar cells are shown in Figure 5A. A 3D structure image of a tandem solar cell measured by Zygo white light interferometer shows the 1.8 μm AlGaAs cell is on the top of Si cell. The tandem solar cell array comprised distributed AlGaAs strips both for four-terminal, as shown in SEM image of Figure 5B, and two-terminal tandem solar cells (Fig. 5C). The optical microscopic image of the finished two-terminal tandem solar cells is shown in Figure 5D, where the trace of AlGaAs strips is clear. An electroluminescence (EL) of the AlGaAs/Si dual-junction tandem solar cell is carried out as shown in Figure S2.

Figure 6A shows the measured external quantum efficiency (EQE) of each junction of the AlGaAs/Si dual-junction tandem solar cell without an antireflection (AR) layer. Considering the small area of the device, the area

of the probing metal pad is excluded from the cell area in the device EQE calculation. The top AlGaAs cell exhibits a response edge of the top cell at 688 nm corresponding to the designed bandgap of 1.8 eV. The response of the bottom Si cell at short wavelength is due to its exposed region between AlGaAs cells as shown in Figure 5B. The AlGaAs/Si dual-junction tandem cells were measured under AM 1.5 solar simulator and the performance of the tandem solar cell and each cell are shown in Figure 6B. The tandem gives an open circuit voltage (V_{oc}) of 1.63 V, a short-circuit current density (J_{sc}) of 11.9 mA/cm^2 , a fill factor (FF) of 65%, and an efficiency of 12.7%. The low fill factor is speculated to be caused by a low shunt resistance, as the low shunt resistance causes power loss in solar cells and induces an alternate current path for the light-generated current, which could degrade the current flowing through the solar cell junction and reduce the voltage across the solar cell. The V_{oc} of the tandem solar cell matches well with the sum of V_{oc} of individual AlGaAs cell (1.18 V) and Si cell (0.45 V). The J_{sc} of the Si cell is a little higher than that of the tandem solar

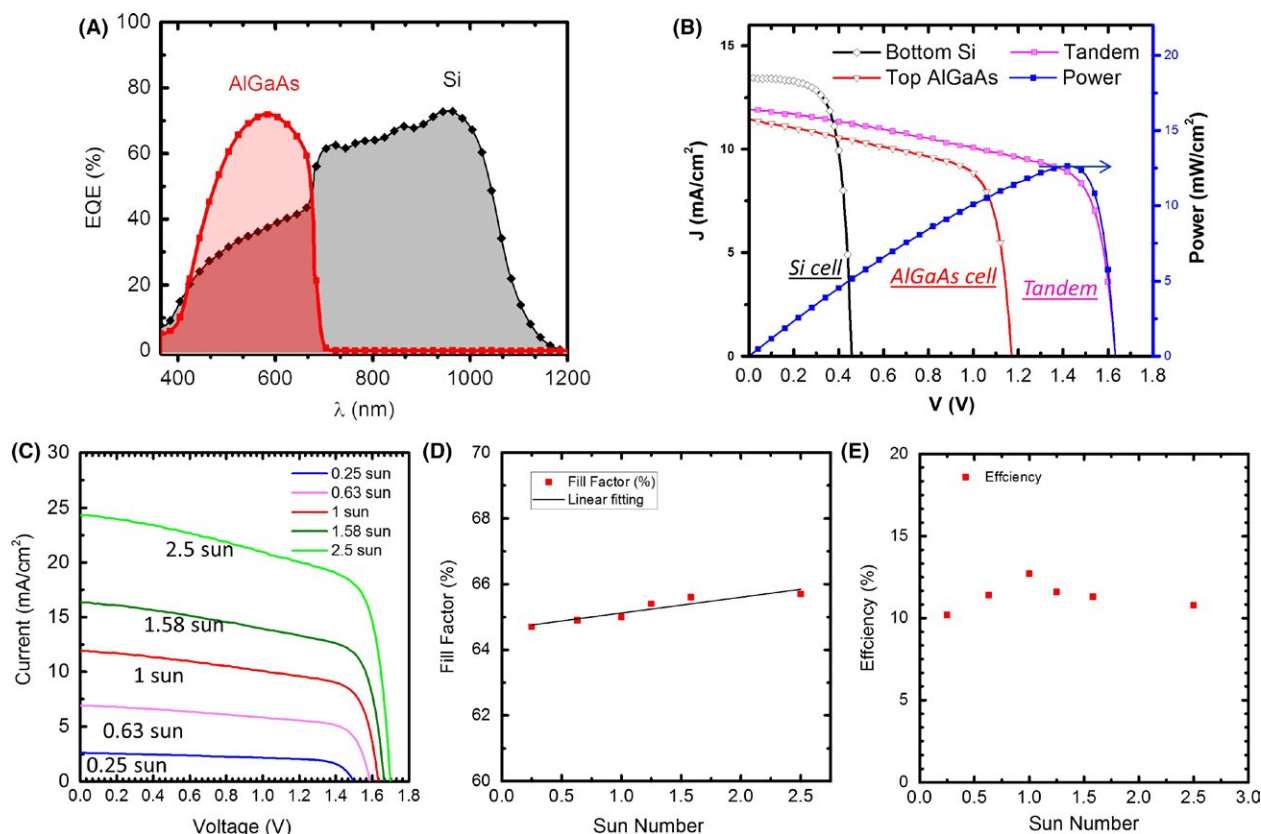


Figure 6. (A) Measured EQE for each junction of the AlGaAs/Si tandem solar cell. (B) Measured current density versus voltage (J-V) characteristics of the AlGaAs/Si tandem solar cell and that of each individual cell under AM 1.5 light illumination. (C) Measured J-V characteristics of the AlGaAs/Si tandem solar cell under different incident light power levels. (D) Fill factor (FF) under different incident light power levels. (E) Measured efficiency of the AlGaAs/Si tandem solar cell under different incident light power levels.

cell. This is because the mesa of the bottom Si cell is on a bulk of Si wafer, which allows the Si cell to collect the lateral current from the region of bulk Si outside the tandem solar cell region. Details of the lateral current collection are shown in Figure S4. It is well demonstrated that, compared to individual cells, the tandem solar cell based on AlGaAs thin film provides better performance. The tests of tandem solar cells under different incident light power densities (0.25 Sun to 2.5 Sun) were also carried out and the resulting I-V curve is shown in Figure 6C. As the incident light power density increases, the V_{oc} , J_{sc} , and FF increase as shown in Figure 6C and D. Meanwhile, the efficiency increases initially (from 0.25 Sun to 1 Sun), and then decreases (from 1 Sun to 2.5 Sun) as shown in Figure 6E, which suggests that the AlGaAs/Si dual-junction tandem work best under the normal sunshine condition.

Conclusion

Using ELO and print-transfer-assisted bonding methods, micrometer-thick AlGaAs films were bonded with Si wafer without the use of bonding agents. The bonding interface is electrically conductive and optically transparent and highly desirable for photovoltaic applications. AlGaAs/Si dual-junction tandem solar cells based on the heterogeneous bonding approach have been demonstrated. The prototype device has shown decent efficiency and an open circuit voltage of 1.63 V under 1 Sun. It is expected that this approach can also be applied to other III-V materials, enabling low cost and highly efficient III-V/Si multijunction solar cells for nonconcentrated photovoltaic applications.

Acknowledgments

The work was supported by AFOSR under a PECASE grant FA9550-09-1-0482. Dr. Gernot Pomrenke is the program manager at AFOSR. K. Xiong, H. Mi, and T.-H. Chang contribute equally to this work. The authors also acknowledge the use of instrumentation supported by NSF MRSEC (DMR-1121288).

Conflict of Interest

None declared.

References

1. Zhang, G., G. Liu, L. Wang, and J. T. S. Irvine. 2016. Inorganic perovskite photocatalysts for solar energy utilization. *Chem. Soc. Rev.* 45:5951–5984.
2. Wang, W., X. Xu, W. Zhou, and Z. Shao. 2017. Recent progress in metal-organic frameworks for applications in

- electrocatalytic and photocatalytic water splitting. *Adv. Sci.* 4:1600371.
3. Lin, C., C. Rüssel, and S. Dai. 2018. Chalcogenide glass-ceramics: functional design and crystallization mechanism. *Prog. Mater. Sci.* 93:1–44.
4. Wang, W., M. O. Tade, and Z. Shao. 2015. Research progress of perovskite materials in photocatalysis- and photovoltaics-related energy conversion and environmental treatment. *Chem. Soc. Rev.* 44:5371–5408.
5. Schnabel, M., T. R. Klein, N. Jain, S. Essig, H. Schulte-Huxel, E. Warren et al. 2017. III-V/Si Tandem cells utilizing interdigitated back contact Si cells and varying terminal configurations: preprint. National Renewable Energy Laboratory (NREL), Golden, CO.
6. Green, M. A., K. Emery, Y. Hishikawa, W. Warta, and E. D. Dunlop. 2015. Solar cell efficiency tables (Version 45). *Prog. Photovoltaics Res. Appl.* 23:1–9.
7. Akiyama, M., Y. Kwarada, and K. Kaminishi. 1984. Growth of GaAs on Si by MOVCD. *J. Cryst. Growth* 68:21–26.
8. Fang, S. F., K. Adomi, S. Iyer, H. Morkoç, H. Zabel, C. Choi et al. 1990. Gallium arsenide and other compound semiconductors on silicon. *J. Appl. Phys.* 68:R31–R58.
9. Soga, T., T. Kato, M. Yang, M. Umeno, and T. Jimbo. 1995. High efficiency AlGaAs/Si monolithic tandem solar cell grown by metalorganic chemical vapor deposition. *J. Appl. Phys.* 78:4196–4199.
10. Dimroth, F., T. Roesener, S. Essig, C. Weuffen, A. Wekkeli, E. Oliva et al. 2014. Comparison of direct growth and wafer bonding for the fabrication of GaInP/GaAs dual-junction solar cells on silicon. *IEEE J. Photovolt.* 4:620–625.
11. Schone, J., F. Dimroth, A. W. Bett, A. Tauzin, C. Jaussaud, and J. C. Roussin. 2006. *III-V solar cell growth on wafer-bonded GaAs/Si-substrates*. Presented at Conference Record of the 2006 IEEE 4th World Conference on Photovoltaic Energy Conversion, May 2006.
12. Archer, M. J., D. C. Law, S. Mesropian, M. Haddad, C. M. Fetzer, A. C. Ackerman et al. 2008. GaInP/GaAs dual junction solar cells on GeSi epitaxial templates. *Appl. Phys. Lett.* 92:103503.
13. Dimroth, F., M. Grave, P. Beutel, U. Fiedeler, C. Karcher, T. N. D. Tibbits et al. 2014. Wafer bonded four-junction GaInP/GaAs//GaInAsP/GaInAs concentrator solar cells with 44.7% efficiency. *Prog. Photovoltaics Res. Appl.* 22:277–282.
14. Liang, J., S. Nishida, M. Morimoto, and N. Shigekawa. 2013. Surface-activating-bonding-based low-resistance Si/III-V junctions. *Electron. Lett.* 49:830–832.
15. Liang, J., T. Miyazaki, M. Morimoto, S. Nishida, N. Watanabe, and N. Shigekawa. 2013. Electrical properties of p-Si/n-GaAs heterojunctions by using surface-activated bonding. *Appl. Phys. Express* 6:021801.

16. Essig, S., O. Moutanabbir, A. Wekkeli, H. Nahme, E. Oliva, A. W. Bett et al. 2013. Fast atom beam-activated n-Si/n-GaAs wafer bonding with high interfacial transparency and electrical conductivity. *J. Appl. Phys.* 113:203512.
17. Derendorf, K., S. Essig, E. Oliva, V. Klinger, T. Roesener, S. P. Philipps et al. 2013. Fabrication of GaInP/GaAs//Si solar cells by surface activated direct wafer bonding. *IEEE J. Photovolt.* 3:1423–1428.
18. Tanabe, K., K. Watanabe, and Y. Arakawa. 2012. III-V/Si hybrid photonic devices by direct fusion bonding. *Sci. Rep.* 2:349.
19. Lin, C.-T., W. E. McMahon, J. S. Ward, J. F. Geisz, M. W. Wanlass, J. J. Carapella et al. 2015. Two-terminal metal-inter-connected multijunction III-V solar cells. *Prog. Photovoltaics Res. Appl.* 23:593–599.
20. Boca, A., J. C. Boisvert, D. C. Law, S. Mesropian, N. H. Karam, W. D. Hong et al. 2010. *Carbon nanotube-composite wafer bonding for ultra-high efficiency III-V multijunction solar cells*. Presented at 2010 35th IEEE Photovoltaic Specialists Conference (PVSC).
21. Schermer, J. J., G. J. Bauhuis, P. Mulder, W. J. Meulemeesters, E. Haverkamp, M. M. A. J. Voncken et al. 2000. High rate epitaxial lift-off of InGaP films from GaAs substrates. *Appl. Phys. Lett.* 76:2131–2133.
22. Lee, K., J. D. Zimmerman, X. Xiao, K. Sun, and S. R. Forrest. 2012. Reuse of GaAs substrates for epitaxial lift-off by employing protection layers. *J. Appl. Phys.* 111:033527.
23. Cheng, C.-W., K.-T. Shiu, N. Li, S.-J. Han, L. Shi, and D. K. Sadana. 2013. Epitaxial lift-off process for gallium arsenide substrate reuse and flexible electronics. *Nat. Commun.* 4:1577.
24. Yablonovitch, E., D. M. Hwang, T. J. Gmitter, L. T. Florez, and J. P. Harbison. 1990. Van der Waals bonding of GaAs epitaxial liftoff films onto arbitrary substrates. *Appl. Phys. Lett.* 56:2419–2421.
25. Sheng, X., C. A. Bower, S. Bonafede, J. W. Wilson, B. Fisher, M. Meitl et al. 2014. Printing-based assembly of quadruple-junction four-terminal microscale solar cells and their use in high-efficiency modules. *Nat. Mater.* 13:593–598.
26. Ahn, J.-H., H.-S. Kim, K. J. Lee, S. Jeon, S. J. Kang, Y. Sun et al. 2006. Heterogeneous three-dimensional electronics by use of printed semiconductor nanomaterials. *Science* 314:1754–1757.
27. Sheng, X., M. H. Yun, C. Zhang, A. A. M. Al-Okaily, M. Masouraki, L. Shen et al. 2015. Device architectures for enhanced photon recycling in thin-film multijunction solar cells. *Adv. Energy Mater.* 5:1400919.
28. van Niftrik, A. T. J., J. J. Schermer, G. J. Bauhuis, P. Mulder, P. K. Larsen, M. J. van Setten et al. 2008. HF species and dissolved oxygen on the epitaxial lift-off process of GaAs using AlAsP release layers. *J. Electrochem. Soc.* 155:D35.
29. Chang, W., C. P. Kao, G. A. Pike, J. A. Slone, and E. Yablonovitch. 1999. Vapor phase epitaxial liftoff of GaAs and silicon single crystal films. *Sol. Energy Mater. Sol. Cells* 58:141–146.
30. Lee, K., J. Lee, B. A. Mazon, and S. R. Forrest. 2014. *Epitaxial lift-off processed GaAs thin-film solar cells integrated with low-cost plastic mini-compound parabolic concentrators*. Presented at Photovoltaic Specialist Conference (PVSC), 2014 IEEE 40th.
31. Vos, D. 1980. Detailed balance limit of the efficiency of tandem solar cells. *J. Phys. D: Appl. Phys.* 13:839–846.

Supporting Information

Additional supporting information may be found in the online version of this article:

Figure S1. The stacked AlGaAs/Si structures.

Figure S2. The p^{++} GaAs/ n^{++} Si conductive heterojunction.

Figure S3. The electroluminescence (EL) of the finished tandem solar cell.

Figure S4. Characterization of the single Si solar cell.